Mineralogical Magazine (2024), **88**, 327–334
doi:10.1180/mgm.2024.16

CAMBRIDGE UNIVERSITY PRESS

Article

Hydroxylbenyacarite, $(H_2O)_2Mn_2(Ti_2Fe)(PO_4)_4[O(OH)](H_2O)_{10}{\cdot}4H_2O$, a new paulkerrite-group mineral, from the El Criollo mine, Cordoba Province, Argentina

Rupert Hochleitner[1], Christian Rewitzer[2], Ian E. Grey[3], Anthony R. Kampf[4], Colin M. MacRae[3], Robert W. Gable[5] and William G. Mumme[3]

[1]Mineralogical State Collection (SNSB), Theresienstrasse 41, 80333, München, Germany; [2]Independent researcher, Furth im Wald, Germany; [3]CSIRO Mineral Resources, Private Bag 10, Clayton South, Victoria 3169, Australia; [4]Mineral Sciences Department, Natural History Museum of Los Angeles County, 900 Exposition Boulevard, Los Angeles, CA 90007, USA; and [5]School of Chemistry, University of Melbourne, Parkville, Victoria 3010, Australia

Abstract

Hydroxylbenyacarite, $(H_2O)_2Mn_2(Ti_2Fe)(PO_4)_4[O(OH)](H_2O)_{10}{\cdot}4H_2O$, is a new paulkerrite-group mineral from the El Criollo mine, Cordoba Province, Argentina (IMA2023–079). It was found in specimens of altered triplite, in association with bermanite, phosphosiderite, quartz, strengite and manganese oxides.

Hydroxylbenyacarite occurs as light greenish-yellow rhombic tablets with dimensions of typically 20 to 50 μm, occasionally to 400 μm. The crystals are flattened on {010}, slightly elongated on [001] and bounded by the {111} and {010} forms. The calculated density is 2.32 g cm^{-3}. Optically, hydroxylbenyacarite crystals are biaxial (+), with $\alpha = 1.608(3)$, $\beta = 1.624(3)$, $\gamma = 1.642(3)$ (measured in white light) and 2V(meas.) = 88(2)°. The calculated 2V is 87.5°. The empirical formula is $Ca_{0.06}\ ^{A}[K_{0.46}(H_2O)_{0.88}\square_{0.66}]_{\Sigma 2.00}\ ^{M1}(Mn_{1.52}Mg_{0.02}Fe^{2+}_{0.35}\square_{0.11})_{\Sigma 2.00}\ ^{M2+M3}(Fe^{3+}_{1.21}Al_{0.02}Ti_{1.77})_{\Sigma 3.00}(PO_4)_4\ ^{X}[F_{0.16}(OH)_{0.70}O_{1.14}]_{\Sigma 2.00}(H_2O)_{10}{\cdot}3.77H_2O$.

The average crystal structure for hydroxylbenyacarite has space group *Pbca* and unit cell parameters $a = 10.5500(3)$ Å, $b = 20.7248(5)$ Å, $c = 12.5023(3)$ Å, $V = 2733.58(12)$ Å^3 and $Z = 4$. It was refined using single-crystal data to $wR_{obs} = 0.074$ for 2611 reflections with $I > 3\sigma(I)$. The crystal structure contains corner-connected linear trimers of Ti-centred octahedra that share corners with PO_4 tetrahedra to form 10-member rings parallel to (010). K^+ cations and water molecules are located in interstitial sites within the rings. Additional corner-sharing of the PO_4 tetrahedra with $MnO_2(H_2O)_4$ octahedra occurs along [010] to complete the 3D framework structure. A new eight-coordinated interstitial site, previously unreported for paulkerrite-group minerals, is occupied by Ca^{2+} cations. Weak diffuse diffraction spots in reconstructed precession images for hydroxylbenyacarite violate the *a* and *b* glide plane extinctions for *Pbca* and are consistent with local, unit-cell-scale regions of monoclinic, $P2_1/c$ structure, in which ordering of the interstitial K^+ and Ca^{2+} cations occurs.

Keywords: hydroxylbenyacarite; new mineral from Argentina; crystal structure; paulkerrite-group member

(Received 11 December 2023; accepted 4 March 2024; Accepted Manuscript published online: 19 March 2024; Associate Editor: Daniel Atencio)

Introduction

Hydroxylbenyacarite was discovered by authors RH and CR in a specimen provided by the late Hebe Dina Gay from the El Criollo mine in the Cerro Blanco Pegmatite District near Tanti, San Roque District, Punila Department, Cordoba Province, Argentina (31°21'28''S, 64°39'09''W). The El Criollo mine is the type locality for benyacarite, $KTiMn_2Fe_2(PO_4)_4(OF){\cdot}15H_2O$ (Demartin *et al.*, 1993, 1997), a member of the paulkerrite group. The formula for benyacarite has recently been revised to $(H_2O)_2Mn_2(Ti_2Fe)(PO_4)_4(OF)(H_2O)_{10}{\cdot}4H_2O$, consistent with the paulkerrite-group nomenclature (Grey *et al.*, 2023a). Preliminary energy-dispersive X-ray analysis of crystals by RH and CR indicated that the mineral corresponded to the hydroxyl analogue of benyacarite, with OH dominant over F, and subsequent electron microprobe analyses (EMPA) and a single-crystal structure refinement confirmed the initial finding. The new mineral hydroxylbenyacarite (symbol Hbyc) was approved by the Commission on New Minerals, Nomenclature and Classification of the International Mineralogical Association (IMA–CNMNC) as IMA2023–079 (Hochleitner *et al.*, 2024). The holotype specimen is housed in the mineralogical collections of the Natural History Museum of Los Angeles County, catalogue number 76298. A cotype specimen is in the Mineralogical State Collection, Munich, registration number MSM 38036.

Occurrence and associated minerals

The hydroxylbenyacarite specimen derives from a granite pegmatite at the El Criollo mine. The pegmatite contains large masses of triplite up to 5 metres. The maroon brown triplite is partially altered to secondary phosphate minerals, especially bluish

Corresponding author: Ian E. Grey; Email: ian.grey@csiro.au
Cite this article: Hochleitner R., Rewitzer C., Grey I.E., Kampf A.R., MacRae C.M., Gable R.W. and Mumme W.G. (2024) Hydroxylbenyacarite, $(H_2O)_2Mn_2(Ti_2Fe)(PO_4)_4[O(OH)](H_2O)_{10}{\cdot}4H_2O$, a new paulkerrite-group mineral, from the El Criollo mine, Cordoba Province, Argentina. *Mineralogical Magazine* **88**, 327–334. https://doi.org/10.1180/mgm.2024.16

phosphosiderite, lilac strengite and reddish-brown bermanite. Other alteration products of triplite at the locality are libethenite, dufrenite, red–brown eosphorite and rockbridgeite-group minerals. The new mineral occurs in corrosion cavities in the triplite, associated with strengite, quartz and fine-grained manganese oxides (Fig. 1). It is younger than the other phosphates.

Physical and optical properties

Hydroxylbenyacarite forms isolated and intergrown light greenish-yellow rhombic tablets. The crystals generally have dimensions of 20 to 80 μm, occasionally up to ~400 μm (Fig. 1). The crystals are flattened on {010} and slightly elongated on [001], with the main forms being {010} and {111}. The calculated density for the empirical formula and single-crystal unit cell volume is 2.32 g cm^{-3}.

Optically, hydroxylbenyacarite crystals are biaxial (+), with $\alpha = 1.608(3)$, $\beta = 1.624(3)$ and $\gamma = 1.642(3)$ (measured in white light). The 2V is 88(2)°, measured directly on a spindle stage, compared with 2V (calc.) = 87.5°. Dispersion is moderate with $r < v$. The optical orientation is $X = \mathbf{b}$, $Y = \mathbf{c}$ and $Z = \mathbf{a}$. The mineral is nonpleochroic. The Gladstone–Dale compatibility index (Mandarino, 1981) is 0.016 (superior) based on the empirical formula and single-crystal unit-cell parameters.

Raman spectroscopy

Raman spectroscopy was conducted on a Horiba XploRA PLUS spectrometer using a 532 nm diode laser, 100 μm slit and 1800gr/mm diffraction grating and a 100× (0.9 NA) objective. The spectrum is shown in Fig. 2. The O–H stretch region has two broad bands with maxima at 3373 and 3101 cm^{-1} and shoulders at 3609, 3481, 3212 and 2958 cm^{-1}. The H–O–H bending mode region for water has a band at 1660 cm^{-1}. The P–O stretching region has a strong band at 949 cm^{-1} with shoulders at 1013 and 980 cm^{-1} corresponding to symmetric P–O stretching modes and a weaker band at 1133 cm^{-1} corresponding to an antisymmetric P–O stretch. Bending modes of the $(PO_4)^{3-}$ groups are manifested by a band centred at 597 cm^{-1} and a composite band with a maximum at 411 cm^{-1} and shoulders at 479 and 445 cm^{-1}. Peaks at lower wavenumbers are related to lattice vibrations. An intense pair of bands at 832 and 774 cm^{-1} is a consistent feature of paulkerrite-group minerals that can be assigned to Ti–O stretching vibrations associated with short Ti–O bonds, as reported for numerous titanates (Bamberger *et al.*, 1990; Tu *et al.*, 1996). Silva *et al.* (2018) have recently reported the modelling of the Raman spectrum of $Na_2Ti_3O_7$ using first-principles calculations based on density functional theory. The spectrum has a strong band at 849 cm^{-1} and a weaker band at 740 cm^{-1} that were assigned as Ti–O stretching modes for Ti–O bonds with distances of 1.76 and 1.85 Å. For comparison, hydroxylbenyacarite has a similar Ti–O distance at the *M*2 site of 1.81 Å that could be associated with the band at 832 cm^{-1}. The peak at 774 cm^{-1} in the Raman spectrum for hydroxylbenyacarite may be the corresponding Ti–F stretching vibrations for Ti at the *M*2 site.

Figure 1. Greenish-yellow crystal of hydroxylbenyacarite associated with lilac strengite and yellowish cryptocrystalline quartz on specimen MSM38036. Minerals below the hydroxylbenyacarite crystal are coated with black manganese oxides. Field of view 1.65 mm. Photo by Christian Rewitzer.

Chemical composition

Crystals of hydroxylbenyacarite were difficult to analyse because they underwent severe cracking due to dehydration resulting from beam heating and the high vacuum of the microprobe. The results presented in Table 1 are for regions of crystals that were least affected by cracking. The crystals were analysed using wavelength-dispersive spectrometry on a JEOL JXA 8500F Hyperprobe operated at an accelerating voltage of 15 kV and a beam current of 2.2 nA. The beam was defocused to 5 μm. Analytical results (average of 5 analyses on 5 crystals) are given in Table 1. There was insufficient material for direct determination of H_2O, of which the presence is indicated by a low analysis total for oxides and confirmed by Raman spectroscopy, so it was based upon the crystal structure, with 15 H_2O per 4 P. The FeO/Fe_2O_3 proportioning in Table 1 is obtained from the crystal structure, with Fe^{2+} at the *M*1 site and Fe^{3+} at the *M*2 and *M*3 sites.

The microprobe analyses showed a small departure (1.222) from the stoichiometric ratio of ΣM/P from the crystal structure of 5/4 = 1.25, and the structure refinement confirmed that metal atom vacancies occurred at the *M*1 site, so the normalisation of the formula was based on 4 P per formula unit, giving the atoms per formula unit as:

$$K_{0.46}Ca_{0.06}Mn_{1.52}Mg_{0.02}Fe^{2+}_{0.34}Fe^{3+}_{1.22}Al_{0.02}Ti_{1.77}P_4F_{0.16}O_{32.48}H_{30}.$$

Expressing the empirical results in structural form gives the empirical formula:

$$Ca_{0.06}\,{}^{A}[K_{0.46}(H_2O)_{0.88}\square_{0.66}]_{\Sigma 2.00}\,{}^{M1}(Mn_{1.52}Mg_{0.02}Fe^{2+}_{0.35}\square_{0.11})_{\Sigma 2.00}\,{}^{M2+M3}(Fe^{3+}_{1.21}Al_{0.02}Ti_{1.77})_{\Sigma 3.00}(PO_4)_4\,{}^{X}[F_{0.16}(OH)_{0.70}O_{1.14}]_{\Sigma 2.00}(H_2O)_{10}\cdot 3.77H_2O.$$

The compositions at the *M*2 and *M*3 sites have been merged so that the end-member composition can be determined using the merged-sites procedure recently approved for paulkerrite-group minerals by the IMA-CNMNC, proposal revised 22-K-bis (Grey *et al.*, 2023a). The merged ($M2_2M3$) sites approach is illustrated graphically in Fig. 3, showing a ternary Al_3–Fe^{3+}_3–Ti_3 diagram with the possible end-member compositions designated (e.g.

https://doi.org/10.1180/mgm.2024.16 Published online by Cambridge University Press

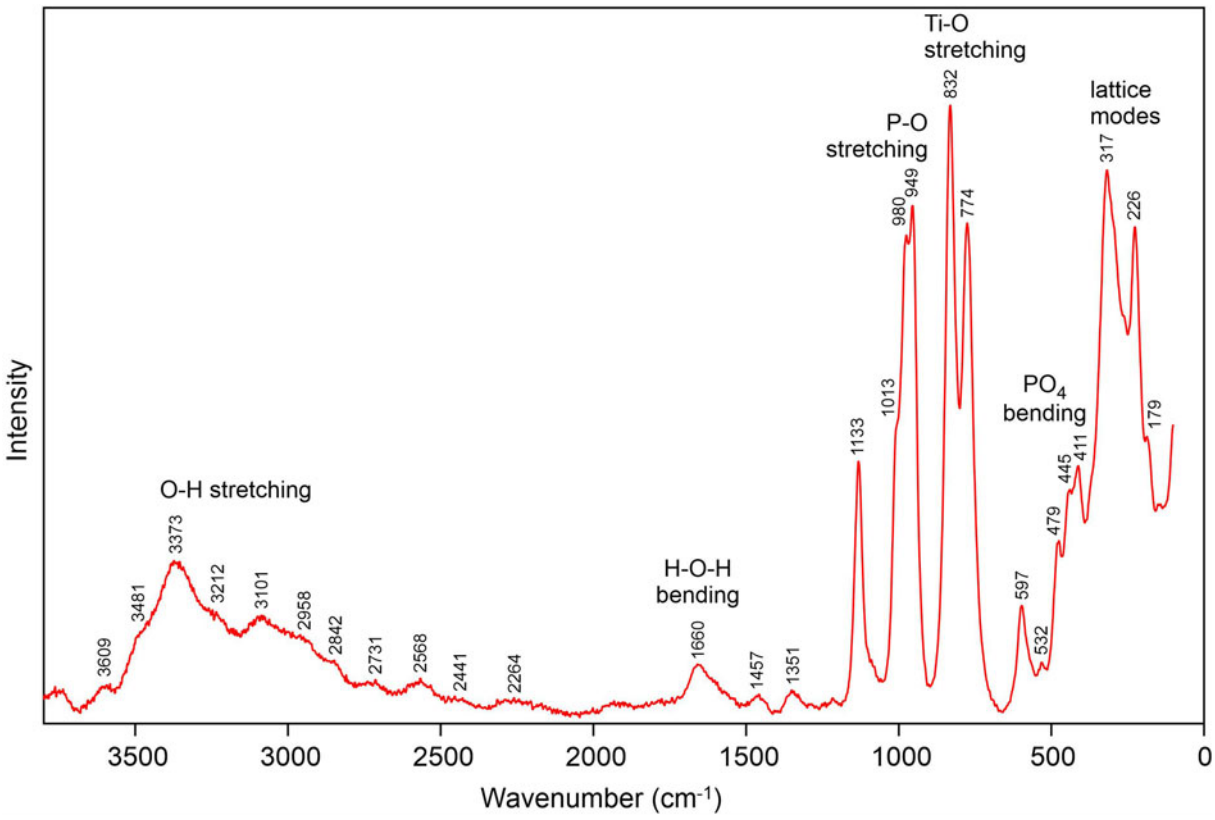

Figure 2. Raman spectrum for hydroxylbenyacarite.

Ti_3, Al_2Ti, $TiFe_2$). The empirical ($M2_2M3$) composition for hydroxylbenyacarite is shown in Fig. 3 to be located in the end-member (Ti_2Fe) composition field. Combining with the dominant constituents at $M1$, A and X sites gives the end-member formula $(H_2O)_2Mn_2(Ti_2Fe)(PO_4)_4[O(OH)](H_2O)_{10}{\cdot}4H_2O$, which requires MnO 14.74, Fe_2O_3 8.30, TiO_2 16.60, P_2O_5 29.50, H_2O 30.86, total 100 wt.%. Note that charge neutrality in the end-member formula requires mixed-valency O^{2-} and OH^-/F^- and OH^- is dominant over F^- (in accord with Hatert and Burke, 2008 and Bosi *et al.*, 2019).

Table 1. Chemical data (wt.%) for hydroxylbenyacarite.

Constituent	Mean	Range	S.D.	Standard
K_2O	2.25	1.90–2.67	0.29	Adularia
CaO	0.36	0.13–1.09	0.41	Wollastonite
MnO	11.11	10.29–12.95	1.06	$MnSiO_3$
MgO	0.07	0.03–0.16	0.06	Spinel
Al_2O_3	0.08	0.02–0.28	0.11	Berlinite
Fe_2O_3 (total)	(12.75)	11.68–14.99	1.34	Hematite
FeO *	2.50			
Fe_2O_3 *	9.98			
TiO_2	14.57	13.35–17.19	1.53	Rutile
P_2O_5	29.17	26.18–33.50	2.86	Berlinite
F	0.32	0.00–0.56	0.18	Fluorite
H_2O_{calc}	27.74			
$-O{\equiv}F$	−0.13			
Total	98.02			

*Fe^{2+}/Fe^{3+} based on the crystal structure, with Fe^{2+} assigned with all Mn^{2+} and Mg at the $M1$ site and the remaining iron as Fe^{3+} assigned to the $M2$ and $M3$ sites.
S.D. – standard deviation

Crystallography

Powder X-ray diffraction data were recorded using a Rigaku R-Axis Rapid II curved imaging plate microdiffractometer with monochromatised Mo$K\alpha$ radiation. A Gandolfi-like motion on the φ and ω axes was used to randomise the sample. Observed d values and intensities were derived by profile fitting using *JADE Pro* software (Materials Data, Inc.). Data are given in

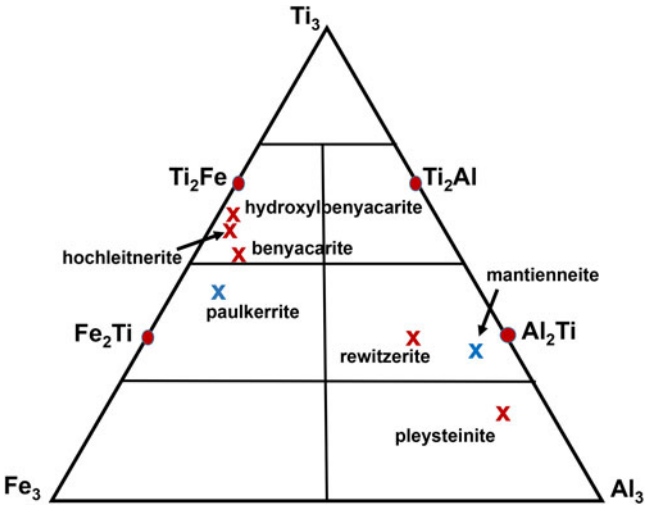

Figure 3. Ternary diagram for ($M2_2M3$) site Al–Ti–Fe^{3+} compositions, showing end-member compositions (e.g. Al_2Ti, $AlTi_2$) and location of the experimental composition for hydroxylbenyacarite and for other published paulkerrite-group minerals. Blue crosses have Mg at $M1$ and red crosses have Mn at $M1$.

https://doi.org/10.1180/mgm.2024.16 Published online by Cambridge University Press

Table 2. Refined orthorhombic unit-cell parameters (space group *Pbca* (#61)) are $a = 10.580(14)$, $b = 20.78(3)$, $c = 12.529(17)$ Å, $V = 2755(7)$ Å^3 and $Z = 4$.

Single-crystal diffraction data were collected on a crystal measuring 0.071 × 0.131 × 0.179 mm. Data were collected at 299 K using a XtaLab Synergy 4-circle diffractometer equipped with a Dualflex Hypix detector and using Mo*K*α radiation, λ = 0.71073 Å. Refined unit-cell parameters and other data collection details are given in Table 3.

Structure refinement in Pbca

A structural model was obtained in space group *Pbca* using *SHELXT* (Sheldrick, 2015). It was found to conform to the general structural formula for orthorhombic paulkerrite-group members, $A_2M1_2M2_2M3(PO_4)_4X_2(H_2O)_{10}{\cdot}4H_2O$, where divalent cations (Mn^{2+}, Mg and Fe^{2+}) are located at *M*1 and Fe^{3+}, Al and Ti are located at the *M*2 and *M*3 sites (Grey *et al.*, 2023a). Using the EMPA as a guide, Mn, Mg and Fe were assigned to *M*1, with the Mn and Mg contents fixed at the empirical formula values and the Fe content refined. Fe and Ti were assigned to *M*2 and *M*3 and the site occupancies of the pair of atoms refined. K and O (for H_2O) were assigned to the *A* site, with the K content fixed at the empirical formula value and the O content refined. For both the *M*1 and *A* sites, less than full occupancy was obtained, corresponding to vacancies at these sites. A difference-Fourier map showed a relatively large peak (2.9 e^- Å^{-3}) at a site coordinated to 8 oxygens at distances in the range 2.23 to 2.72 Å, mean value 2.52 Å. The coordination number and bond lengths are consistent with Ca which was present as a minor constituent in the chemical analyses. With Ca located at the site, its occupancy refined to a value within the spread of CaO analyses (Table 1). The refinement was conducted using anisotropic displacement parameters (ADPs) for all atoms except the partially occupied Ca site. Two oxygen atoms (O4 and O5) were found to have slightly non-positive definite ADPs, and the displacement parameters were made isotropic for these atoms, Details of the data collection and refinement are given in Table 3. The refined coordinates, equivalent isotropic displacement parameters and bond valence sum (BVS) values (Gagné and Hawthorne, 2015) are reported in Table 4. Selected interatomic distances are reported in Table 5. Although H atoms were not located in the refinement, the BVS values in Table 4 show clearly the presence of seven independent H_2O groups, O9 to O15, as well as an anion site, *X*, having a low BVS of 1.66 due to partial incorporation of OH as indicated in the empirical formula. The crystallographic information file has been deposited with the Principal Editor of *Mineralogical Magazine* and is available as Supplementary material (see below).

Table 2. Powder X-ray diffraction data (*d* in Å) for hydroxylbenyacarite (I_{calc} > 1.5), *Pbca* model.*

I_{obs}	d_{obs}	d_{calc}	I_{calc}	*h k l*	I_{obs}	d_{obs}	d_{calc}	I_{calc}	*h k l*
48	**10.48**	10.3624	71	0 2 0	17	2.356	2.3659	6	4 2 2
71	**7.56**	7.5143	70	1 1 1			2.3339	9	1 8 2
85	**6.28**	6.2512	100	0 0 2	8	2.205	2.2001	3	4 4 2
		5.3780	3	1 0 2			2.1908	2	4 5 1
50	**5.28**	5.2750	34	2 0 0			2.1475	3	2 3 5
		5.1812	16	0 4 0			2.1218	2	2 6 4
19	4.73	4.7734	2	1 2 2	13	2.095	2.0963	3	4 6 0
		4.7010	6	2 2 0			2.0837	10	0 0 6
		4.0314	2	2 0 2	31	1.9965	2.0157	5	4 0 4
29	4.008	3.9750	28	2 3 1			1.9875	21	4 6 2
		3.8099	3	1 1 3			1.9785	3	3 8 2
52	**3.763**	3.7571	38	2 2 2	17	1.9487	1.9630	3	5 2 2
		3.7313	2	1 4 2			1.9454	3	4 7 1
		3.6964	4	2 4 0	21	1.9288	1.9332	8	0 4 6
		3.4541	2	0 6 0			1.9050	8	2 2 6
		3.3803	4	1 3 3	10	1.8837	1.8748	8	5 1 3
		3.1817	2	2 4 2			1.8656	2	2 8 4
100	**3.157**	3.1538	54	2 5 1	7	1.8541	1.8595	2	5 5 1
		3.1256	24	0 0 4			1.8432	5	2 10 2
16	3.042	3.0650	9	3 0 2	6	1.7947	1.7927	7	3 0 6
		3.0399	2	3 3 1			1.7806	4	4 7 3
		3.0233	8	0 6 2	11	1.7343	1.7410	3	4 6 4
13	2.980	2.9968	15	1 0 4			1.7271	10	0 12 0
		2.9556	4	2 3 3			1.7182	3	4 9 1
		2.9391	4	3 2 2			1.7023	2	5 7 1
38	**2.892**	2.8897	20	2 6 0	10	1.6975	1.6941	3	3 4 6
		2.8789	8	1 2 4			1.6901	7	2 6 6
12	2.813	2.8311	13	1 5 3			1.6861	2	2 1 7
		2.6890	5	2 0 4	20	1.6692	1.6725	2	1 9 5
		2.6763	2	0 4 4			1.6651	11	6 4 0
36	**2.643**	2.6380	13	3 4 2	8	1.6443	1.6413	4	2 12 0
		2.6230	16	2 6 2			1.6296	3	4 10 0
		2.6028	2	2 2 4	16	1.6174	1.6208	3	1 5 7
20	2.580	2.5941	6	1 4 4			1.6150	6	4 2 6
		2.5609	13	4 1 1			1.6090	4	6 4 2
18	2.537	2.5285	13	2 7 1			1.6015	2	4 9 3
		2.5048	6	3 3 3	12	1.5713	1.5769	7	4 10 2
		2.4165	2	1 1 5			1.5704	2	5 3 5
		2.3867	3	2 4 4			1.5670	2	6 6 0

*Strongest reflections shown in bold font.

Table 3. Crystal data and *Pbca* crystal structure refinement for hydroxylbenyacarite.

Formula from refinement	$K_{0.47}Ca_{0.06}Mn_{1.53}Ti_{1.78}Fe_{1.55}Mg_{0.01}P_4O_{33}$
Formula weight	954.3
Temperature	299 K
Wavelength	0.71073 Å
Space group	*Pbca* (#61)
Unit cell dimensions	$a = 10.5500(3)$ Å
	$b = 20.7248(5)$ Å
	$c = 12.5023(3)$ Å
Volume	2733.59(12) Å^3
Z	4
Absorption correction	Gaussian, $\mu = 2.43$ mm^{-1}
Crystal size	0.071 × 0.131 × 0.179 mm
Theta range for data collection	2.55 to 31.84°
Index ranges	$-14 \le h \le 15$
	$-30 \le k \le 29$
	$-15 \le l \le 18$
Reflections collected	44408
Independent reflections	3961 ($R_{int} = 0.088$)
Reflections with $I_o > 3\sigma(I)$	2611
Refinement method	Full-matrix least-squares on *F*
Data / restraints / parameters	3961 / 0 / 195
Final *R* indices [$I > 3\sigma(I)$]	$R_{obs} = 0.074$, *wR_{obs} = 0.099
R indices (all data)	$R_{obs} = 0.112$, w$R_{obs} = 0.106$
Goodness of Fit	2.73
Largest diff. peak and hole	1.17 and −1.24 *e*.Å^{-3}

*$w = [\sigma^2(|F_o|)+(uF_o)^2]^{-1}$, u = instability factor

Structure refinement in P2$_1$/c

In the processing of the single-crystal data using *CrysAlisPro* (Rigaku OD, 2022), automatic data reduction chose the orthorhombic cell given in the previous section, with parameters obtained from the fitting of 18,367 reflections, but the program also provided an unconstrained triclinic unit cell with parameters

https://doi.org/10.1180/mgm.2024.16 Published online by Cambridge University Press

Table 4. Atomic coordinates, equivalent isotropic displacement parameters (Å^2) and bond valence sums (BVS, in valence units) for hydroxylbenyacarite, *Pbca* average structure.

	Occupancy	*x*	*y*	*z*	U_{eq}	BVS
*M*1	0.77Mn+0.01Mg+0.123(5)Fe	0.49554(8)	0.74821(4)	0.24602(8)	0.0189(3)	1.86
*M*2	0.69(2)Ti+0.31Fe	0.65952(7)	0.50141(4)	0.74174(6)	0.0142(2)	3.72
*M*3	0.65(3)Ti+0.35Fe	½	½	½	0.0162(3)	3.63
P1		0.90987(11)	0.59430(6)	0.80136(9)	0.0103(3)	5.01
P2		0.58774(12)	0.59150(6)	0.29772(10)	0.0148(4)	5.06
A	0.23K+0.46(1)O	0.7177(4)	0.85512(18)	0.0586(3)	0.0391(13)	0.17
Ca	0.073(6)Ca	0.4871(13)	0.8317(6)	−0.0081(11)	0.017(5)*	0.14
X		0.6434(3)	0.50180(17)	0.5975(3)	0.0149(8)	1.66
O1		0.9049(4)	0.66691(17)	0.8038(4)	0.0264(12)	1.74
O2		1.0253(3)	0.56930(16)	0.7390(3)	0.0175(10)	1.80
O3		0.9099(3)	0.56849(17)	0.9178(2)	0.0165(10)	1.88
O4		0.7887(3)	0.56893(15)	0.7463(3)	0.0138(7)*	1.89
O5		0.5953(3)	0.66512(17)	0.2950(3)	0.0184(8)*	1.65
O6		0.4661(4)	0.56872(17)	0.2386(3)	0.0197(10)	1.79
O7		0.5840(3)	0.56812(17)	0.4126(3)	0.0197(10)	1.94
O8		0.7055(4)	0.56501(19)	0.2428(3)	0.0273(12)	1.89
O9		0.3458(4)	0.6859(2)	0.1781(4)	0.0321(13)	0.29
O10		0.5880(5)	0.7430(2)	0.0796(4)	0.0366(14)	0.29
O11		0.6445(4)	0.8090(2)	0.3119(5)	0.0383(15)	0.32
O12		0.4082(4)	0.7525(2)	0.4071(4)	0.0393(15)	0.34
O13		0.6598(4)	0.4985(2)	0.9158(3)	0.0296(12)	0.34
O14		0.2606(4)	0.6423(2)	0.4396(3)	0.0337(14)	0.02
O15		0.5288(7)	0.4036(3)	1.0119(5)	0.072(3)	0.02

*U_{iso}

$a = 10.5512(2)$, $b = 20.7276(5)$, $c = 12.4988(3)$ Å, $\alpha = 90.027(2)$, $\beta = 90.065(2)$ and $\gamma = 89.99(2)°$. Although a satisfactory refinement of the crystal structure was obtained in an orthorhombic cell, space group *Pbca*, as for benyacarite (Demartin *et al.*, 1993) the β value of 90.065° prompted an exploration of the possibility of the structure having monoclinic symmetry, analogous to the $P2_1/c$ structures for other paulkerrite-group minerals (Grey *et al.*, 2023a). It was possible to obtain a constrained monoclinic cell in *CrysAlisPro*, with $a = 10.5467(3)$, $b = 20.7222(5)$, $c = 12.5031(3)$ Å, $\alpha = 90$, $\beta = 90.068(2)$ and $\gamma = 90°$. To further check on the possibility of lower symmetry, simulated precession images were generated from the complete diffraction data using the *UNWARP* facility in the *CrysAlisPro* software. The **a***b* zone is shown in Fig. 4 for two different scalings. Fig. 4a shows that the pattern contains diffuse streaking parallel to **b***, suggestive of (010) stacking faults, as has been reported for paulkerrite (Peacor *et al.*, 1984). In Fig. 4b the scale was increased to emphasise weaker diffraction effects. This image shows diffuse reflections with $h = 2n+1$ that violate the *a*-glide extinction conditions for *Pbca*. Similarly, the **b***c* zone showed very weak diffuse reflections with $k = 2n + 1$ that are not allowed in *Pbca*. On the basis of these observations, we converted the *Pbca* model coordinates to those for the $P2_1/c$ subgroup in *JANA2006* (Petříček *et al.*, 2014) and refined the monoclinic model. The refinement was problematic, in giving numerous non-positive ADPs and relatively wide ranges of P–O distances, 1.48 to 1.58 Å. Nevertheless, an important result from the $P2_1/c$ refinement was that not only does some K/H_2O ordering occur in split *A* sites as reported for other monoclinic paulkerrite-group members (Grey *et al.*, 2023a), but Ca was also ordered in only one of the two sites generated by transformation of the *Pbca* structure.

The refinement difficulties encountered in the $P2_1/c$ refinement are most likely linked to the structural disorder that is indicated by the streaking parallel to **b*** and to the diffuse nature of the weak reflections. Based on the lengths of the diffuse streaks, the Ca and K/H_2O ordering that is associated with the symmetry lowering is restricted to domains on the scale of the unit cell, 1 to 2 nm. In the absence of better-quality crystals of hydroxylbenyacarite, we restrict our discussion of the crystal structure to the orthorhombic representation in *Pbca*, which corresponds to the average structure. Further analysis of the structural disorder evidenced by the streaked reflections shown in Fig. 4 may benefit from the modular approach described by Aksenov *et al.* (2023).

Table 5. Polyhedral bond lengths [Å] for *the Pbca* model for hydroxylbenyacarite.

P1–O1	1.506(4)	P2–O5	1.528(4)
P1–O2	1.536(4)	P2–O6	1.554(4)
P1–O3	1.551(3)	P2–O7	1.517(4)
P1–O4	1.545(3)	P2–O8	1.522(4)
<P1–O>	1.535	<P2–O>	1.530
*M*1–O1	2.097(4)	*A*–*X*	3.105(5)
*M*1–O5	2.109(4)	*A*–O4	2.922(5)
*M*1–O9	2.210(4)	*A*–O7	2.802(5)
*M*1–O10	2.301(5)	*A*–O10	2.710(6)
*M*1–O11	2.177(4)	*A*–O12	2.957(6)
*M*1–O12	2.216(5)	*A*–O15	2.916(8)
<M1–O>	2.185	<*A*–O,*X*>	2.902
*M*2–*X*	1.811(3)	Ca–*A*	2.617(14)
*M*2–O2	2.011(3)	Ca–O1	2.697(15)
*M*2–O4	1.954(3)	Ca–O3	2.493(14)
*M*2–O6	1.982(4)	Ca–O5	2.715(14)
*M*2–O8	1.980(4)	Ca–O7	2.518(14)
*M*2–O13	2.177(4)	Ca–O10	2.390(14)
<M2–O,*X*>	1.986	Ca–O12	2.206(14)
		Ca–O14	2.536(14)
*M*3–*X* ×2	1.944(3)	<Ca–O,*A*>	2.522
*M*3–O3 ×2	1.994(3)		
*M*3–O7 ×2	1.993(4)		
<M3–O,*X*>	1.977		

https://doi.org/10.1180/mgm.2024.16 Published online by Cambridge University Press

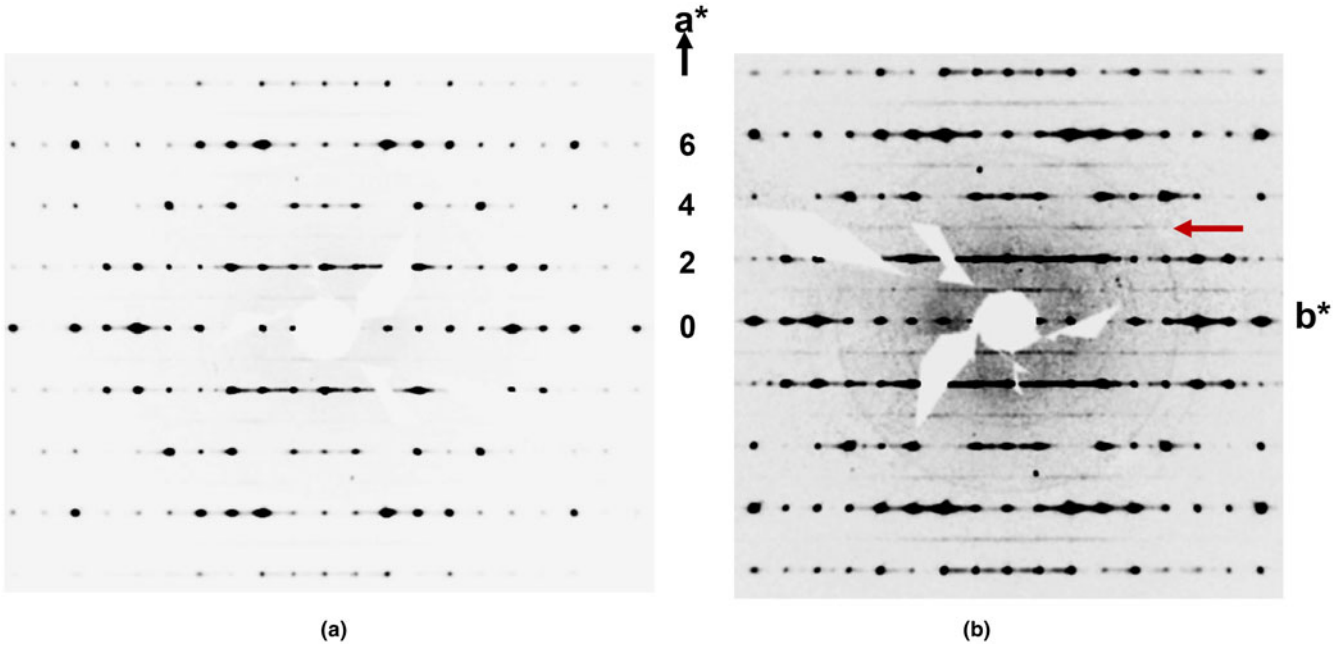

Figure 4. Reconstructed **a***__b__* precession images generated at two different scale values (a) shows diffuse streaking parallel to **b***, indicative of (010) stacking faults. (b) A higher scale was employed to show weak diffraction effects. Weak diffuse reflections with $h = 2n + 1$, as indicated by the red arrow, violate the *a*-glide extinction condition for *Pbca* but are consistent with subgroup $P2_1/c$.

Discussion

The hydroxylbenyacarite average crystal structure in *Pbca* is built from an alternation of two types of (001) slabs, centred at $z = ¼$, ¾ and 0, ½. These are shown in Figs 5 and 6, respectively. The heteropolyhedral layers at $z = ¼$, ¾ contain [100] kröhnkite-type chains (Hawthorne, 1985) of four-member rings of corner-connected PO_4 tetrahedra and $M2O_4X(H_2O)$ octahedra. Each PO_4 tetrahedron also shares a corner with $M1O_2(H_2O)_4$ octahedra along [010] to complete the 2D network of polyhedra. The corner-shared linkages form eight-member rings of alternating octahedra and tetrahedra. The (001) slabs at $z = 0$, ½ comprise isolated $M3O_4X_2$ octahedra together with Ca, the *A* site constituents (K, H_2O) and the zeolitic-type H_2O groups at sites O14 and O15. The Ca site has not been previously reported in crystal structure studies of other paulkerrite-group members. As seen in Fig. 6, one of the Ca bonds is to H_2O at the *A* site (labelled as K).

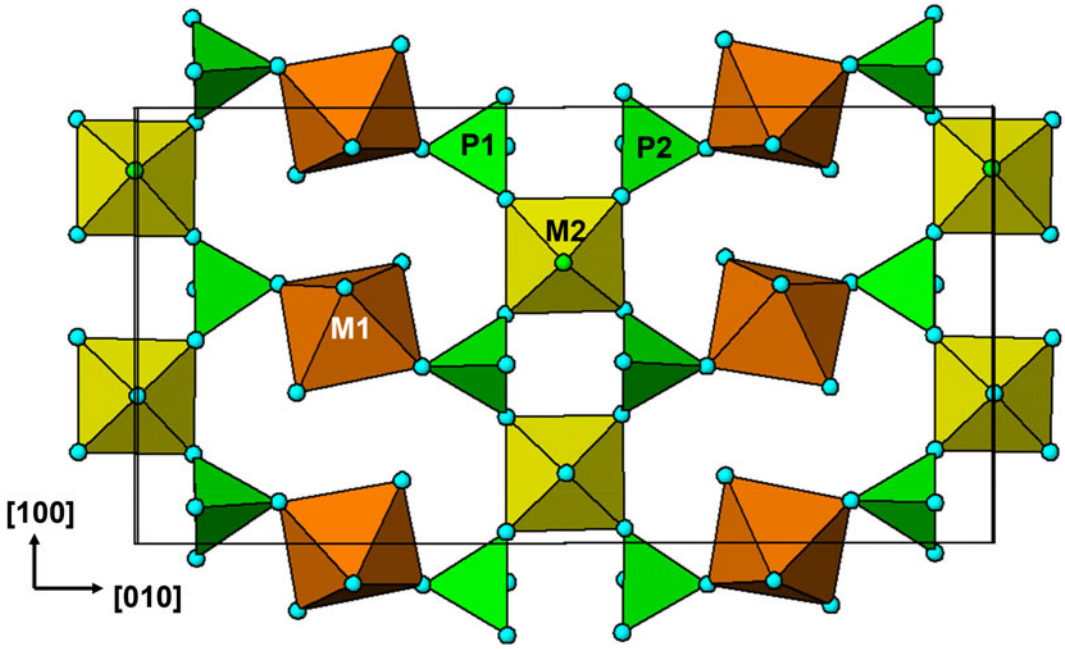

Figure 5. (001) section of the hydroxylbenyacarite structure at $z = ¼$. Drawn using *ATOMS* (Dowty, 2004).

https://doi.org/10.1180/mgm.2024.16 Published online by Cambridge University Press

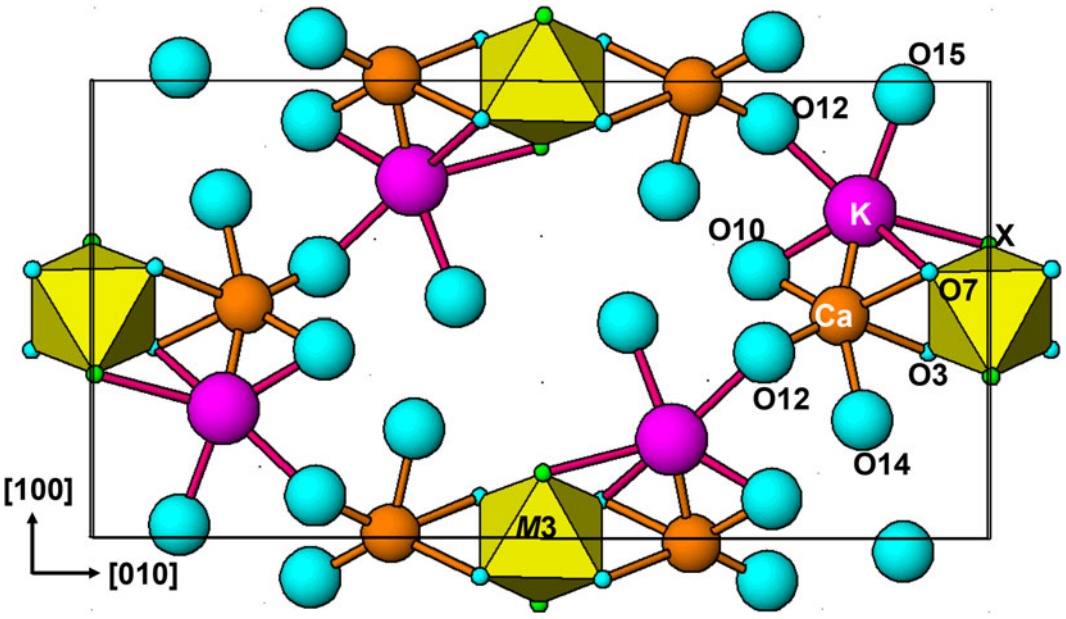

Figure 6. (001) section of the hydroxylbenyacarite structure at $z = 0$, showing in-section bonds to Ca and K. Drawn using *ATOMS* (Dowty, 2004).

The distance Ca–*A* is only 2.62 Å, so occupations of the Ca site and of K at the *A* site are mutually exclusive. Locally, when Ca is present, the *A* site is occupied by H_2O. The Ca-centred polyhedron has 12 triangular faces in the form of a snub disphenoid deltahedron.

The $M3O_4X_2$ octahedra share their *trans*-X vertices with $M2O_4X(H_2O)$ octahedra in the layers above and below, giving linear trimers that correspond to short segments of the 7 Å chains that are common to many phosphate minerals (Moore, 1970). The *M*2–*M*3–*M*2 trimers are illustrated in Fig. 7. A feature of the trimers is a short *M*2–*X* distance (1.81 Å), due to displacement of the *M*2-site atoms from the centres of the octahedra towards the bridging *X*-site anions with the *M*3-centred octahedra. This type of displacement is a common feature of chain structures containing Ti (Bamberger *et al.*, 1990) and is the origin of the strong Raman bands in the region 770–850 cm^{-1} (Fig. 2). The corner-shared connectivity between the kröhnkite-type chains and the $M3O_4X_2$ octahedra (Fig. 7) generates 10-member rings, elongated along [100]. The water molecules at O14 and O15 and the *A*-site constituents, K and H_2O, are located at interstitial sites within the ring whereas the Ca site is at the periphery.

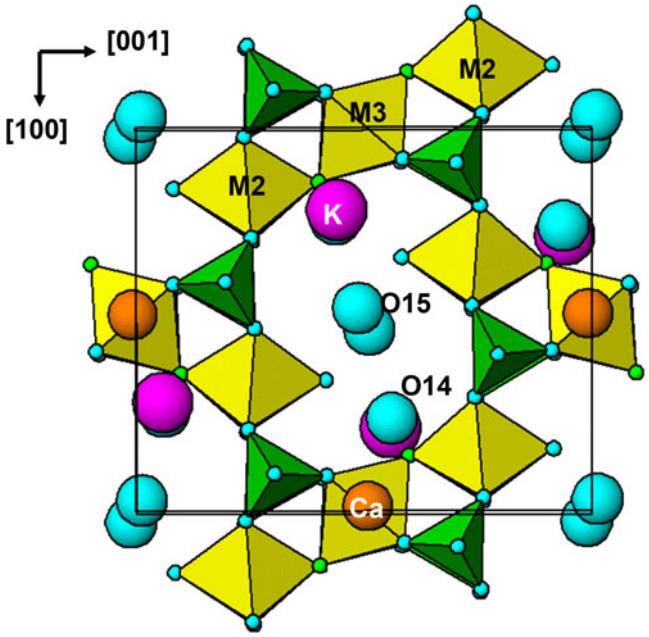

Figure 7. (010) section through the structure of hydroxylbenyacarite at $y = 0$. Drawn using *ATOMS* (Dowty, 2004).

Based on the presence of weak diffuse diffraction effects such as shown in Fig. 4, hydroxylbenyacarite has monoclinic symmetry, space group $P2_1/c$, with ordering of the interstitial K^+ and Ca^{2+} cations, though the ordering is restricted to very small regions on the scale of the unit cell. Locally, hydroxylbenyacarite has the same symmetry as the monoclinic paulkerrite-group minerals rewitzerite (Grey *et al.*, 2023b), paulkerrite (Grey *et al.*, 2023a) and macraeite (Bosi *et al.*, 2023). The other group members are the orthorhombic minerals benyacarite (Demartin *et al.*, 1993, 1997) and mantienneite (Fransolet *et al.*, 1984), and the minerals pleysteinite (Grey *et al.*, 2023c) and hochleitnerite (Grey *et al.*, 2023d). The latter two minerals were reported as orthorhombic, *Pbca*, isostructural with benyacarite, based on laboratory single-crystal diffraction data. However the diffraction patterns of these minerals are affected by sectoral twinning, and new (Rewitzer *et al.*, 2024) data collections using a synchrotron microfocus source to obtain data from a single sector, have shown that both pleysteinite and hochleitnerite are monoclinic, $P2_1/c$, isostructural with paulkerrite.

The general formulae are $A_2M1_2M2_2M3(PO_4)_4X_2(H_2O)_{10}{\cdot}4H_2O$ for orthorhombic members and $A1A2M1_2M2_2M3(PO_4)_4X_2(H_2O)_{10}{\cdot}4H_2O$ for monoclinic members, where $A = K$, H_2O and □ (= vacancy); $M1 = Mn^{2+}$, Mg, Fe^{2+}, Zn and Ca (rarely Fe^{3+}); *M*2 and $M3 = Fe^{3+}$, Al and Ti^{4+}; and $X = O$, OH and F. In monoclinic species, K and H_2O show an ordering at the *A*1 and *A*2 sites. The end-member formulae for the members, and their unit-cell parameters are reported in Table 6. The formulae are based on the merged ($M2_2M3$) site compositions approach that has

https://doi.org/10.1180/mgm.2024.16 Published online by Cambridge University Press

Table 6. Paulkerrite-group members*.

Mineral	Formula	Unit-cell parameters	Refs.
Hydroxylbenyacarite	$(H_2O)_2Mn_2(Ti_2Fe)(PO_4)_4[O(OH)](H_2O)_{10}{\cdot}4H_2O$	*Pbca*, *a* = 10.5500(3), *b* = 20.7248(5), *c* = 12.5023(3) Å	[1av]
		$P2_1/c$, *a* = 10.5467(3), *b* = 20.7222(5), *c* = 12.5031(3) Å, β = 90.068(2)	[1]
Benyacarite	$(H_2O)_2Mn_2(Ti_2Fe)(PO_4)_4(OF)(H_2O)_{10}{\cdot}4H_2O$	*Pbca*, *a* = 10.561(5), *b* = 20.585(8), *c* = 12.516(2) Å	[2]
Mantienneite	$(H_2O)_2Mg_2(Al_2Ti)(PO_4)_4(OH)_2(H_2O)_{10}{\cdot}4H_2O$	*Pbca*, *a* = 10.409(2), *b* = 20.330(4), *c* = 12.312(2) Å	[3]
Rewitzerite	$K(H_2O)Mn_2(Al_2Ti)(PO_4)_4[O(OH)](H_2O)_{10}{\cdot}4H_2O$	$P2_1/c$, *a* = 10.444(2), *b* = 20.445(2), *c* = 12.269(1) Å, β = 90.17(3)°	[4]
Paulkerrite	$(H_2O)KMg_2(Fe_2Ti)(PO_4)_4(OF)(H_2O)_{10}{\cdot}4H_2O$	$P2_1/c$, *a* = 10.569(2), *b* = 20.590(4), *c* = 12.413(2) Å, β = 90.33(3)°	[5]
Hochleitnerite	$[(H_2O)K]Mn_2(Ti_2Fe)(PO_4)_4O_2(H_2O)_{10}{\cdot}4H_2O$	*Pbca*, *a* = 10.5513(3), *b* = 20.6855(7), *c* = 12.4575(4) Å	[6]
		$P2_1/c$, *a* = 10.547(2), *b* = 20.577(4), *c* = 12.373(2) Å, β = 90.09(3)°	**
Pleysteinite	$[(H_2O)K]Mn_2Al_3(PO_4)_4F_2(H_2O)_{10}{\cdot}4H_2O$	*Pbca*, *a* = 10.4133(8), *b* = 20.5242(17), *c* = 12.2651(13) Å	[7]
		$P2_1/c$, *a* = 10.440(5), *b* = 20.588(5), *c* = 12.234(2) Å, β = 90.38(1)°	**
Macraeite	$[(H_2O)K]Mn_2(Fe_2Ti)(PO_4)_4[O(OH)](H_2O)_{10}{\cdot}4H_2O$	$P2_1/c$, *a* = 10.562(2), *b* = 20.725(4), *c* = 12.416(2) Å, β = 90.09(3)°	[8]

*Formulae are based on the merged ($M2_2M3$) site compositions approach as approved by the IMA–CNMNC, nomenclature proposal revised 22-K-bis.
**Monoclinic unit cells for pleysteinite and hochleitnerite obtained from synchrotron microfocus beam diffraction studies (Rewitzer *et al.*, 2024).
References: [1] This work; [1av] average local structure; [2] Demartin *et al.* (1993); [3] Fransolet *et al.* (1984); [4] Grey *et al.* (2023b); [5] Grey *et al.* (2023a); [6] Grey *et al.* (2023d); [7] Grey *et al.* (2023c); [8] Bosi *et al.* (2023)]

been approved by the IMA-CNMNC, nomenclature proposal revised 22_K-bis (Grey *et al.*, 2023a). As seen from Table 6, hydroxylbenyacarite is the hydroxyl analogue of benyacarite. It is also closely related to hochleitnerite, having the same dominant constituents at *M*1 (Mn) and at the merged ($M2_2M3$) site (Ti_2Fe) but different dominant constituents at the *A* and *X* sites.

Acknowledgements. Thanks to Cameron Davidson for sample preparation for EMP analyses.

Supplementary material. The supplementary material for this article can be found at https://doi.org/10.1180/mgm.2024.16.

Competing interests. The authors declare none.

References

Aksenov S.M., Charkin D.O., Banaru A.M., Banaru D.A., Volkov S.N., Deineko D.V., Kuznetsov A.N., Rastsvetaeva R.K., Chukanov N.K., Shkurskii B.B. and Yamnova N.A. (2023) Modularity, polytypism, topology, and complexity of crystal structures of inorganic compounds (review). *Journal of Structural Chemistry*, **64**, 1797–2028.

Bamberger C.E., Begun G.M. and MacDougall C.S. (1990) Raman spectroscopy of potassium titanates: Their synthesis, hydrolytic reactions and thermal stability. *Applied Spectroscopy*, **44**, 31–37.

Bosi F., Hatert F., Halenius U., Pasero M., Ritsuro M. and Mills S.J. (2019) On the application of the IMA-CNMNC dominant-valency rule to complex mineral compositions. *Mineralogical Magazine*, **83**, 627–632.

Bosi F., Hatert F., Pasero M. and Mills S.J. (2023) IMA Commission on New Minerals, Nomenclature and Classification (CNMNC)-Newsletter 76, IMA no. 2023-065. *European Journal of Mineralogy*, **35**, 1073–1078.

Demartin F., Pilati T., Gay H.D. and Gramaccioli C.M. (1993) The crystal structure of a mineral related to paulkerrite. *Zeitschrift fur Kristallographie*, **208**, 57–71.

Demartin F., Gay H.D. Gramaccioli C.M. and Pilati T. (1997) Benyacarite, a new titanium-bearing phosphate mineral species from Cerro Blanco, Argentina. *The Canadian Mineralogist*, **35**, 707–712.

Dowty E. (2004) *ATOMS for Windows, vsn 6.1*. Shape Software.

Fransolet A.-M., Oustriere P., Fontan F. and Pillard F. (1984) La mantiennéite, une novelle espèce minérale du gisement de vivianite d'Anloua, Cameroun. *Bulletin de Mineralogie*, **107**, 737–744.

Gagné O.C. and Hawthorne F.C. (2015) Comprehensive derivation of bond-valence parameters for ion pairs involving oxygen. *Acta Crystallographica*, **B71**, 562–578.

Grey I.E., Boer S., MacRae C.M., Wilson N.C., Mumme W.G. and Bosi F. (2023a) Crystal chemistry of type paulkerrite and establishment of the paulkerrite group nomenclature. *European Journal of Mineralogy*, **35**, 909–919.

Grey I.E., Hochleitner R., Kampf A.R., Boer S., MacRae C.M., Mumme W.G. and Keck E. (2023b) Rewitzerite, $K(H_2O)Mn_2(Al_2Ti)(PO_4)_4[O(OH)](H_2O)_{10}{\cdot}4H_2O$, a new monoclinic paulkerrite-group mineral, from the Hagendorf Süd pegmatite, Oberpfalz, Bavaria, Germany. *Mineralogical Magazine*, **87**, 830–838.

Grey I.E., Hochleitner R., Rewitzer C., Kampf A.R., MacRae C.M., Gable R.W., Mumme W.G., Keck E. and Davidson C. (2023c) Pleysteinite, $(H_2O)_{0.5}K_{0.5}]_2Mn_2Al_3(PO_4)_4F_2(H_2O)_{10}{\cdot}4H_2O$, the Al analogue of benyacarite, from the Hagendorf Sud pegmatite, Oberpfalz, Bavaria, Germany. *European Journal of Mineralogy*, **35**, 189–197.

Grey I.E., Keck E., Kampf A.R., MacRae C.M., Gable R.W., Mumme W.G., Glenn A.M. and Davidson C. (2023d) Hochleitnerite, $[K(H_2O)]Mn_2(Ti_2Fe)(PO_4)_4O_2(H_2O)_{10}{\cdot}4H_2O$, a new paulkerrite-group mineral, from the Hagendorf-Süd pegmatite, Oberpfalz, Bavaria, Germany. *European Journal of Mineralogy*, **35**, 635–643.

Hatert F. and Burke E.A.J. (2008) The IMA–CNMNC dominant-constituent rule revisited and extended. *The Canadian Mineralogist*, **46**, 717–728.

Hawthorne F.C. (1985) Towards a structural classification of minerals: The $^{vi}M^{iv}T_2\Phi_n$ minerals. *American Mineralogist*, **70**, 455– 473.

Hochleitner R., Rewitzer C., Grey I.E., Kampf A.R., MacRae C.M., Gable R.W. and Mumme W.G. (2024) Hydroxylbenyacarite, IMA 2023-079. CNMNC Newsletter 76. *Mineralogical Magazine*, **88**, https://doi.org/10.1180/mgm.2023.89

Mandarino J.A. (1981) The Gladstone-Dale relationship: Part IV. The compatibility concept and its application. *The Canadian Mineralogist*, **19** 441–450.

Moore P.B. (1970) Crystal chemistry of the basic iron phosphates. *American Mineralogist*, **55**, 135–169.

Peacor D.R., Dunn P.J. and Simmons W.B. (1984) Paulkerrite a new titanium phosphate from Arizona. *The Mineralogical Record*, **15**, 303–306.

Petříček V., Dušek M. and Palatinus L. (2014) Crystallographic Computing System JANA2006: General features. *Zeitschrift fur Kristallographie*, **229**, 345–352.

Rewitzer C., Hochleitner R., Grey I.E., Macrae C.M., Mumme W.G., Boer S., Kampf A.R. and Gable R.W. (2024) Monoclinic pleysteinite and hochleitnerite from the Hagendorf Sud pegmatite. *The Canadian Journal of Mineralogy and Petrology*, **62**. https://doi.org/103749/2400003

Rigaku OD (2022) *CrysAlisPro 1.171.42.72a*. Rigaku Oxford Diffraction, UK.

Sheldrick G.M. (2015) Crystal-structure refinement with SHELX. *Acta Crystallographica*, **C71**, 3–8.

Silva F.L.R., Filho A.A.A., Silva M.B., Balzuweit K., Bantiignies J-L., Caetano E.W.S., Moreira R.L., Freire V.N. and Righi A. (2018) Polarized Raman, FTIR, and DFT study of $Na_2Ti_3O_7$ microcrystals. *Journal of Raman Spectroscopy*, **49**, 535–548.

Tu C.-S., Guo A.R., Tao R., Katiyar R.S., Guo R. and Bhalla A.S. (1996) Temperature dependent Raman scattering in $KTiOPO_4$ and $KTiOAsO_4$ single crystals. *Journal of Applied Physics*, **79**, 3235–3240.